Transition Metal Chemistry (2019) 44:663–670
https://doi.org/10.1007/s11243-019-00331-5

Influence of hydrothermal synthesis temperature on the redox and oxygen mobility properties of manganese oxides in the catalytic oxidation of toluene

Xuejun Zhang[1] · Heng Zhao[1] · Zhongxian Song[2] · Jinggang Zhao[1] · Zi'ang Ma[1] · Min Zhao[1] · Yun Xing[1] · Peipei Zhang[3] · Noritatsu Tsubaki[3]

Received: 21 March 2019 / Accepted: 29 April 2019 / Published online: 7 May 2019

Abstract
A series of MnO_x samples synthesized by hydrothermal methods at different temperatures were investigated as catalysts for the oxidation of toluene. The optimum oxidation performance was achieved with the catalyst prepared at 120 °C (Mn-120), for which complete conversion of toluene was attained at 250 °C. The Mn-120 sample possessed the highest concentration of Mn^{3+} and the highest initial H_2 consumption rate, which are indicative of abundant crystal defects and superior reducibility. In addition, Mn-120 exhibited excellent oxidation ability due to the abundance of lattice oxygen species and excellent oxygen mobility. Therefore, the superior catalytic performance of Mn-120 could be attributed mainly to its redox performance and abundant crystal defects, both of which are determined by the temperature of the hydrothermal synthesis of MnO_x.

Introduction

In recent years, volatile organic compounds (VOCs) such as toluene and benzene have been identified as major air pollutants which are hazardous for the environment and human health [1, 2]. Various technologies have been explored for the control of VOCs. Among these, physical absorption technology suffers from low efficiency, while photocatalytic oxidation is associated with higher cost due to the need for ultraviolet light. Meanwhile, thermal incineration technology requires high operating temperatures. Therefore, catalytic oxidation is regarded as a promising approach because of its low cost, high efficiency and low environmental impact [3–5]. The research and development of high efficiency catalysts are the current focus of this technology. Noble metal catalysts (such as Pt and Pd) with high catalytic activities have been widely adopted; however, high cost, easy sintering and sensitivity to poisons all limit their application [6, 7]. In contrast, transition metal and lanthanide oxides (Co, Mn, Ce, etc.) have attracted much effort to identify catalysts with high activity, superior stability, low cost and environmentally friendly nature.

Among the transition metal oxides, manganese oxides (MnO_x) have been considered as an outstanding alternative to noble metal catalysts for the catalytic oxidation of VOCs because of their low-temperature catalytic activity and good redox performance [8]. The methodology for catalyst synthesis is an important factor that can affect the surface properties, morphology, redox performance and catalytic activity of MnO_x materials [9, 10]. Wang et al. [11] observed that a rod-like MnO_2 catalyst prepared by hydrothermal methods exhibited superior catalytic activity for combustion of toluene. During the preparation of catalysts by hydrothermal methods, different conditions (including reaction time and temperature) will lead to obvious changes in catalytic performance of the catalyst. Cheng et al. [12] reported that various well-defined morphologies of α-MnO_2 were obtained under different hydrothermal conditions, giving a variety of catalytic activities in the combustion of dimethyl ether. Likewise, Liao et al. [13] obtained a similar result for MnO_x

✉ Zhongxian Song
songzhongxian@126.com

1 College of Environmental and Safety Engineering, Shenyang University of Chemical Technology, Shenyang 110142, People's Republic of China

2 Faculty of Environmental and Municipal Engineering, Henan Key Laboratory of Water Pollution Control and Rehabilitation Technology, Henan University of Urban Construction, Pingdingshan 467036, People's Republic of China

3 Department of Applied Chemistry, School of Engineering, University of Toyama, Gofuku 3190, Toyama 930-8555, Japan

catalysts with different hydrothermal synthesis times, which showed significant differences in catalytic oxidation of toluene. It has been reported that redox properties are key factors that influence the oxidation activity of manganese oxide catalysts [14]. Sun et al. [15] revealed that strong oxidation capacity can offer high catalytic performance. In addition, Piumetti et al. [16] found that variation in the method of synthesis had obvious effects on the performance of MnO_x catalysts, while Tang et al. [17] reported that MnO_x-based catalysts with different calcination temperatures exhibited various microstructures and oxidation abilities. Likewise, Li et al. [5] observed that doping with other metals could significantly improve the catalytic oxidation of toluene by MnO_x-based catalysts. Therefore, many research groups have adopted the method of varying the preparation conditions to optimize the performance of MnO_x catalysts. However, relatively few studies have explored the effect of hydrothermal synthesis temperature on MnO_x catalysts.

Based on the above considerations, we have investigated the effects of different hydrothermal synthesis temperatures on the redox properties, morphology and texture of MnO_x catalysts. The structure–activity relationships between the microproperties and the catalytic activities were further elaborated by means of several characterization methods, which can guide the further development and elucidation of the mechanism of catalytic oxidation of VOCs such as toluene.

Experimental

Chemicals and materials

All the reagents for the preparation of catalysts were A.R. grade and used as received without any purification. Manganese(II) nitrate, glucose, ammonium carbonate and acrylic acid were purchased from Shenyang Lab Science and Trade Co., Ltd. (Shenyang, China).

Catalyst preparation

In a typical synthesis, glucose (1.81 g, 10 mmol) was dissolved in deionized water (25 mL). Acrylic acid (1.08 g, 15 mmol) was then added, while vigorously stirring for 30 min. $Mn(NO_3)_2$ (8.23 g, 23 mmol) was then dissolved in the mixture. Saturated aqueous $(NH_4)_2CO_3$ was slowly added until the pH of the solution reached 9.0. After stirring at room temperature for 5 h, the solution was transferred to a 100-mL Teflon-lined stainless steel autoclave and kept at different temperatures (100 °C, 120 °C, 140 °C and 180 °C) for 12 h. In each case, the resulting precipitate was washed with deionized water and ethanol and then dried overnight at 105 °C. Finally, the product was calcinated at 550 °C in air for 5 h. The samples were denoted as Mn-X, where X was the hydrothermal synthesis temperature.

Catalyst characterization

Powder X-ray diffraction (XRD) patterns were obtained within the 2θ range of 10°–70° with a constant step of 0.02° 2θ and a counting time of 3 s per step, using a Bruker D8 Advance diffractometer equipped with a Cu K_α X-ray source ($\lambda = 1.54184$ Å).

Raman spectroscopy was carried out with a Renishaw inVia 2000 Raman microscope (Renishaw plc, UK) equipped with an Ar^+ ion laser at 532 nm to assess the graphitic structures of the samples.

Scanning electron microscopy (SEM) experiments were carried out with a cold field emission scanning electron microscope (Hitachi-SU8010).

An ESCALAB 250 photoelectron spectrometer (Thermo Fisher Scientific, USA) with a monochromatized microfocused Al K_α X-ray source ($\lambda = 1.54184$ Å) was used for X-ray photoelectron spectroscopy (XPS) measurements. Charge effects of the samples were corrected by setting the binding energy of adventitious carbon (C1 s) at 284.6 eV.

H_2 temperature-programmed reduction (H_2-TPR) temperature experiments were carried out on a chemisorption instrument (Beijing Builder Electronic Technology Company, PCA-1200). A measured amount of sample (20 mg) was placed in a U-type quartz tube and pretreated in a pure N_2 stream. The temperature was increased to 300 °C at a rate of 10 °C/min for 60 min and then cooled down to 100 °C. The sample was then reduced with an Ar gas mixture containing 5 vol% H_2 at a flow rate of 30 mL/min. Simultaneously, H_2 consumption was recorded by a thermal conductivity detector, while the temperature was gradually elevated to 900 °C. In a typical calculation, the differential area of the thermal conductivity detector (TCD) signal (a_i) was calculated with Eq. (1), where I_i and Δt represent the intensity of the TCD signal and the time interval, respectively. The accumulated area (A_i) was obtained from Eq. (2) where t_i is the accumulated time. The coefficient (f) between the peak area and the amount of H_2 consumption was obtained from the relationship between the H_2 amount in the pulse loop and average area value. Therefore, the total amount of H_2 consumption (X_i) at a certain time was calculated by Eq. (3), and the rate of H_2 consumption (r_i) was obtained by differentiation of X_i as in Eq. (4). Finally, the portion of the H_2 consumption data less than 20% was selected to avoid the influence of structure transformation during reduction.

$$a_i = \frac{1}{2} \times \left(I_i + I_{i+1}\right) \times \Delta t \quad (1)$$

$$A_i = \sum_{t=0}^{t=i} a_i \tag{2}$$

$$X_i = A_i \times f \tag{3}$$

$$r_i = \frac{\mathrm{d}X_i}{\mathrm{d}t} \tag{4}$$

In order to certify the binding capacity of the samples for oxygen, O_2 temperature-programmed desorption (O_2-TPD) was performed with a chemisorption instrument (Beijing Builder Electronic Technology Company, PCA-1200). A 200-mg sample was pretreated with pure He gas at 300 °C for 60 min. The sample was then cooled down to 50 °C, and an He gas mixture with 20 vol% O_2 blown through the sample at a rate of 30 mL/min for 60 min. Finally, the sample was heated under pure He to 900 °C.

Catalytic activity evaluation

The catalytic activity for oxidation of toluene was determined using a fixed-bed reactor (i.d. = 8 mm, o.d. = 10 mm), in which 0.1 mL of catalyst (40–60 mesh) was loaded. Catalytic activity was measured over the temperature of 180–300 °C, and the temperature was obtained with a K-type thermocouple in the quartz tube. In the tests, the feed was set with a toluene concentration of 500 ppm, using a flowing N_2 mixture containing 20 vol% O_2 with a total flow rate of 100 mL/min. The concentration of toluene in the inlet and outlet gases was measured with an online FULI 9790 II gas chromatograph equipped with FID detectors. In order to avoid deviations caused by gas adsorption, all the tests were started after running the reaction for 30 min. The toluene conversion was calculated using Eq. (5):

$$\text{Toluene conversion} = \frac{C_{*\text{Toluene}} - C_{\text{Toluene}}}{C_{*\text{Toluene}}} \times 100\% \tag{5}$$

In this equation, $C_{*\text{Toluene}}$ refers to the inlet concentration of toluene and C_{Toluene} is the outlet concentration.

The toluene oxidation was also characterized by CO_2 generation, Eq. (6):

$$CO_2 \text{ generation} = \frac{C_{CO_2}}{C_{*CO_2}} \times 100\% \tag{6}$$

where C_{*CO_2} is the concentration of CO_2 in the effluent when toluene is oxidized completely and C_{CO_2} is the value at different temperatures.

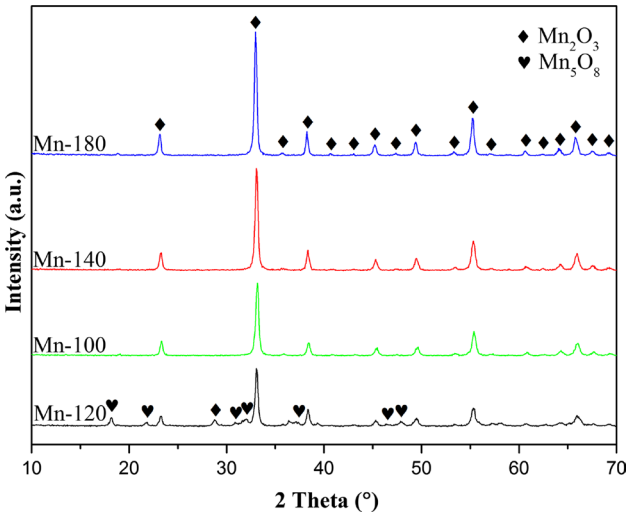

Fig. 1 XRD patterns of the Mn-100, Mn-120, Mn-140 and Mn-180 catalysts

Results and discussion

Material textural properties

The XRD patterns of the prepared catalysts are depicted in Fig. 1. All of the samples showed the reflections typical of Mn_2O_3 [16] at 23.1, 32.9, 38.2, 45.2, 49.3, 55.2 and 65.8° (PDF-# 41-1442). Peaks corresponding to Mn_5O_8 [18] were also apparent for the Mn-120 sample. Qi et al. [18] have previously suggested that the presence of Mn_5O_8 would facilitate redox reactions. The intensities of the diffraction peaks for the Mn-140 and Mn-180 samples were stronger than the others, probably resulting from the growth of crystals at the relatively high hydrothermal synthesis temperatures used to prepare these samples. The crystallite sizes of the different samples were calculated and ranked as follows: Mn-120 (26.9 nm) < Mn-100 (28.2 nm) < Mn-140 (32.8 nm) < Mn-180 (34.2 nm). As reported by Hu [19], smaller particle size is conducive to reduction reactions on the catalyst, which can contribute to the catalytic performance [20].

The Mn-X catalysts were examined by Raman spectroscopy to explore their microstructures. Figure 2 shows the Raman spectra of these Mn-X catalysts in the range of 300–900 cm^{-1}. For all four samples, a main band was observed at 619 cm^{-1}. This can be assigned to the asymmetric stretching mode of bridging oxygen species (Mn–O–Mn), arising from Mn_2O_3 moieties [21, 22]. The Raman spectrum of Mn-120 was clearly broader, with dramatically decreased peak intensities, compared to the other samples. These observations can be attributed to more lattice defects, probably due to the exposure of high-energy surfaces [1]. Hence,

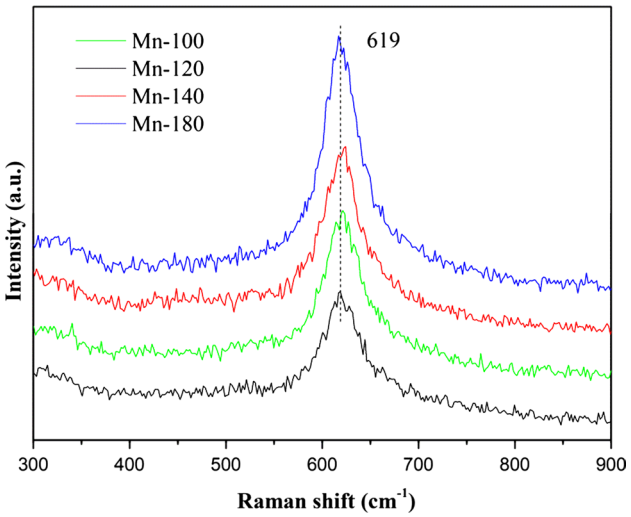

Fig. 2 Raman spectra of the Mn-100, Mn-120, Mn-140 and Mn-180 catalysts

the degree of crystallization depended on the hydrothermal synthesis temperature.

The morphologies of the different MnO_x catalysts were investigated by SEM techniques, and the resulting images are shown in Fig. 3. The microstructures of all four samples were relatively regular, and the overall shape of the nanoparticles was spherical. When the hydrothermal synthesis temperature was lower (Mn-100 and Mn-120), the resulting microspheres were smaller. At higher synthesis temperatures, the aggregation of MnO_x particles was observed. Hence, the agglomeration of the spherical structure in Mn-140 was more pronounced and the microspheres were larger, which was not conducive to exposure of the active sites. When the hydrothermal synthesis temperature reached 180 °C, the distance between nanoparticles increased and the microspheres became loose. Therefore, the microstructure of the catalysts would deteriorate at higher hydrothermal synthesis temperatures.

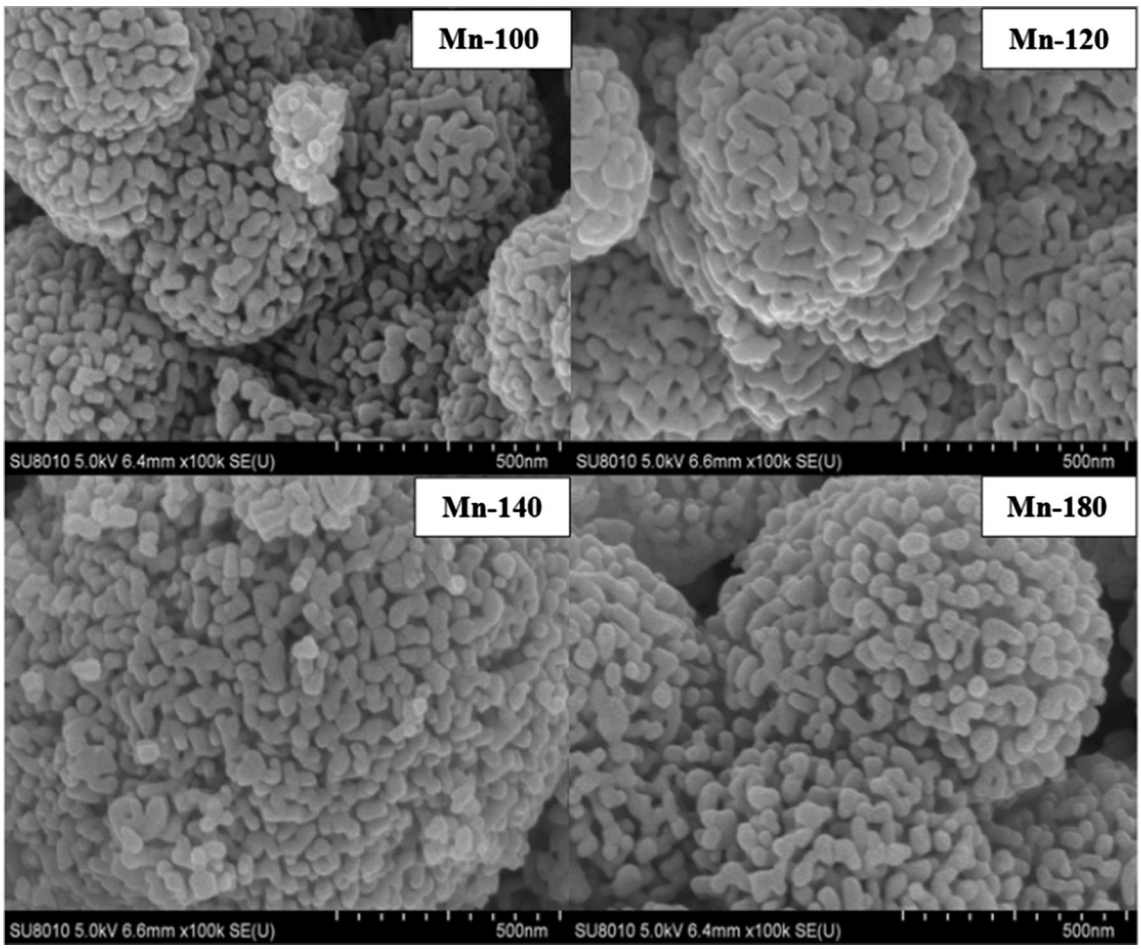

Fig. 3 SEM images of the Mn-100, Mn-120, Mn-140 and Mn-180 catalysts

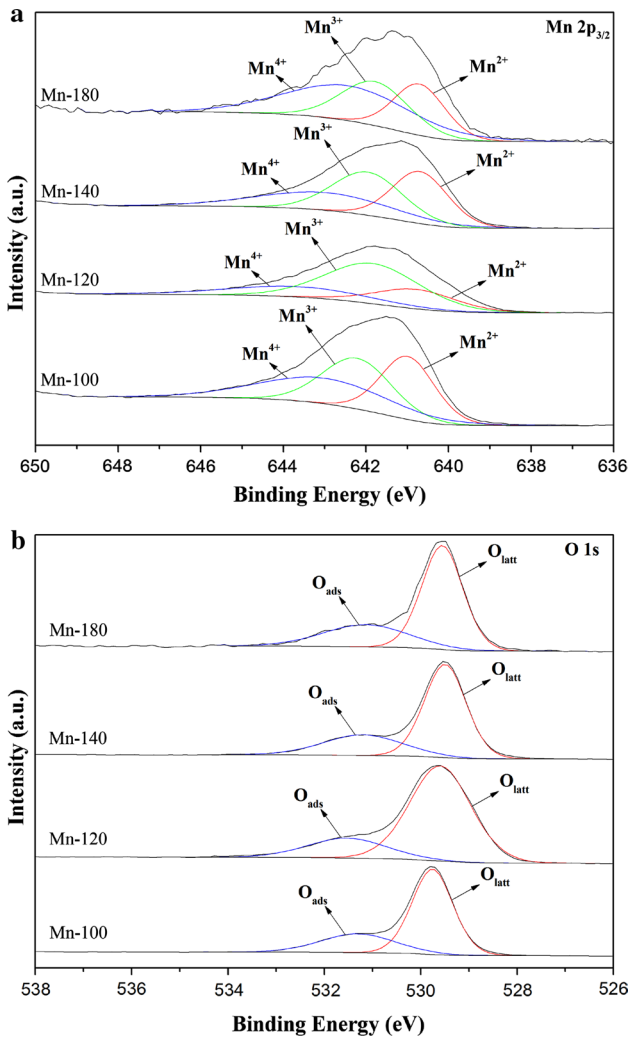

Fig. 4 Mn $2p_{3/2}$ XPS (**a**) and O 1s XPS (**b**) spectra of the Mn-100, Mn-120, Mn-140 and Mn-180 catalysts

Spectroscopic characterization

In order to further investigate the surface composition of the catalysts, XPS experiments were performed and the results are shown in Fig. 4 and Table 1. As shown in Fig. 4a, a main peak was observed and assigned to Mn $2p_{3/2}$ at 636–650 eV. The peak could be further resolved into three components with binding energies (BE) centered at 642.4–643.6, 641.8–642.2 and 640.7–641.0 eV, which are assigned to Mn^{4+}, Mn^{3+} and Mn^{2+}, respectively [10, 16, 23]. As reported in Table 1, the highest Mn^{3+}/Mn^{n+} ratio (0.56) was attained for the Mn-120 sample. Conversely, the ratios for Mn-100 (0.34), Mn-140 (0.36) and Mn-180 (0.30) were much lower than for Mn-120. According to the findings of Santos [24], Mn^{3+} has a weak binding capacity for oxygen. Likewise, Yu et al. [25] reported that higher Mn^{3+}/Mn^{n+} ratios lead to an increase in both oxygen vacancies and crystal defects, with associated enhancement of the redox properties. Hence, Mn-120 would be expected to have the best catalytic activity.

Figure 4b illustrates the oxygen 1s profiles of these Mn-X catalysts. The spectra show different features, depending on both the adsorbed oxygen (O_{ads}) and the lattice oxygen (O_{latt}). Thus, the peaks at 529.5–529.8 eV correspond to O_{latt}, while the signals at 531.2–531.5 eV can be attributed to O_{ads} [26]. The surface element molar ratios O_{ads}/O_{latt} were calculated and are given in Table 1. Generally speaking, oxidation reactions on MnO_x catalysts proceed by the Mars-Van Krevelen (MvK) mechanism, in which the oxidation ability of the catalyst is very important [27]. Lee et al. [28] determined that MnO_2 samples with greater amounts of lattice oxygen species exhibit better oxidation ability than Mn_2O_3 in the oxidation of NO to NO_2. Hence, in the present case, the Mn-120 sample with the highest concentration of lattice oxygen should possess the strongest oxidation ability.

Temperature-programmed studies

In order to further characterize the redox properties of the four catalysts, a series of temperature-programmed studies were performed. H_2-TPR experiments were conducted in order to investigate the reducibility of the four samples, and the results are presented in Fig. 5. All of the curves show two main peaks around 310 and 410 °C, corresponding to the reduction in MnO_2 to Mn_2O_3 and Mn_2O_3 to MnO, respectively [29]. In addition, there is an obscure peak below 200 °C, which can be assigned to the reduction in the oxygen species at the catalyst's surface. Compared to the other three samples Mn-100 (313 °C), Mn-140 (313 °C) and Mn-180 (315 °C), the initial reduction temperature of Mn-120 (308 °C) is lower. Furthermore, the curve for Mn-120 showed an obvious shoulder around 267 °C, indicating that

Table 1 Binding energies and surface atomic ratios from XPS of the Mn-100, Mn-120, Mn-140 and Mn-180 catalysts

Catalysts	Mn^{4+} Be (eV)	Mn^{3+} Be (eV)	Mn^{2+} Be (eV)	O_{ads} Be (eV)	O_{latt} Be (eV)	Mn^{3+}/Mn^{n+}	O_{ads}/O_{latt}
Mn-100	643.0	642.2	641.0	531.3	529.8	0.34	0.41
Mn-120	643.6	641.8	640.8	531.5	529.6	0.56	0.27
Mn-140	643.0	642.0	640.7	531.2	529.5	0.36	0.42
Mn-180	642.4	641.8	640.8	531.2	529.6	0.30	0.44

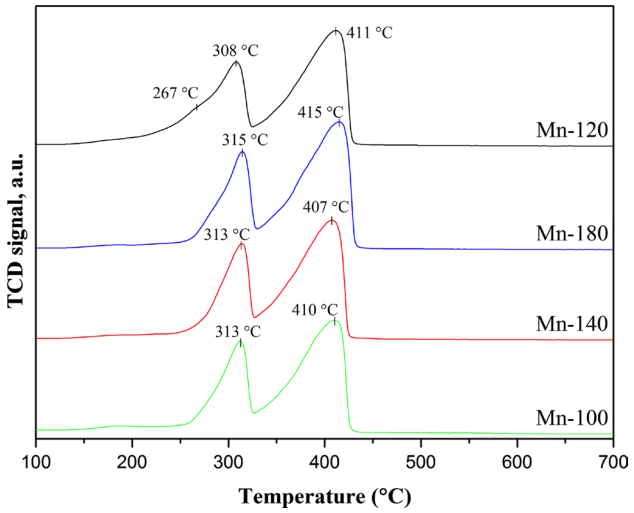

Fig. 5 H_2-TPR patterns of the Mn-100, Mn-120, Mn-140 and Mn-180 catalysts

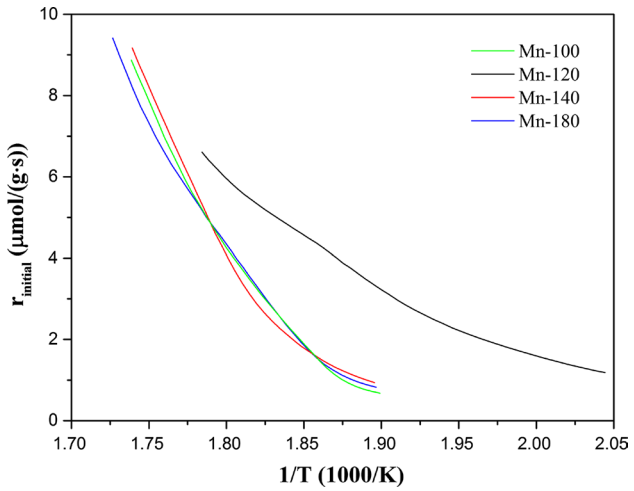

Fig. 6 Initial H_2 consumption rates at low temperature of the Mn-100, Mn-120, Mn-140 and Mn-180 catalysts

the Mn-120 started to reduce at a lower temperature. In fact, the reaction of oxygen species with H_2 at low temperature (below 400 °C) is related to catalytic performance, which is reflected in the low-temperature reducibility [30]. Therefore, the total amount of H_2 consumption and the initial H_2 consumption rate ($r_{Initial}$) at low temperature were calculated for each catalyst. The order of total H_2 consumption was: Mn-120 (8.19 mmol/g) > Mn-140 (7.44 mmol/g) > Mn-100 (7.42 mmol/g) = Mn-180 (7.42 mmol/g), indicating that Mn-120 possessed the highest content of reducible oxygen species. As shown in Fig. 6, Mn-120 exhibited the highest initial H_2 consumption rate at the same temperature.

Table 2 Catalytic activities of the Mn-100, Mn-120, Mn-140 and Mn-180 catalysts

Catalyst	Activity (°C)	
	T_{50}/T^{a}_{*50}	T_{90}/T^{b}_{*90}
Mn-100	241/242	248/251
Mn-120	235/236	247/248
Mn-140	239/241	249/253
Mn-180	243/244	250/255

[a]T_{50} means the temperature of conversion of toluene reached 50%, and T_{*50} means the temperature of yield of CO_2 reached 50%

[b]T_{90} means the temperature of conversion of toluene reached 90%, and T_{*90} means the temperature of yield of CO_2 reached 90%

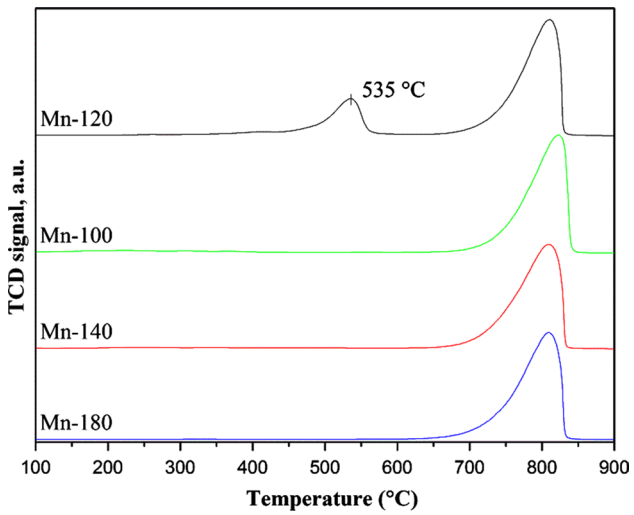

Fig. 7 O_2-TPD patterns of the Mn-100, Mn-120, Mn-140 and Mn-180 catalysts

These phenomena are all indications of the superior redox properties of Mn-120. Clearly, the hydrothermal synthesis temperature has an important effect on the properties of the catalyst (Table 2).

The type and mobility of the oxygen species were further investigated by O_2-TPD. As shown in Fig. 7, all four catalysts exhibited a minor peak below 400 °C and a stronger peak around 800 °C, which can be assigned to the desorption of surface chemisorbed oxygen and bulk lattice oxygen species [1], respectively. It is worth noting that Mn-120 showed an additional peak corresponding to the desorption of the surface lattice oxygen species at 535 °C [1]. Comparing the desorption curves, Mn-120 exhibited the best mobility of the lattice oxygen. According to the XPS results, the abundant Mn^{3+} sites on the surface of Mn-120 are most likely responsible for its high oxygen mobility, due to the weak binding capacity to oxygen. Oxygen mobility is one of the

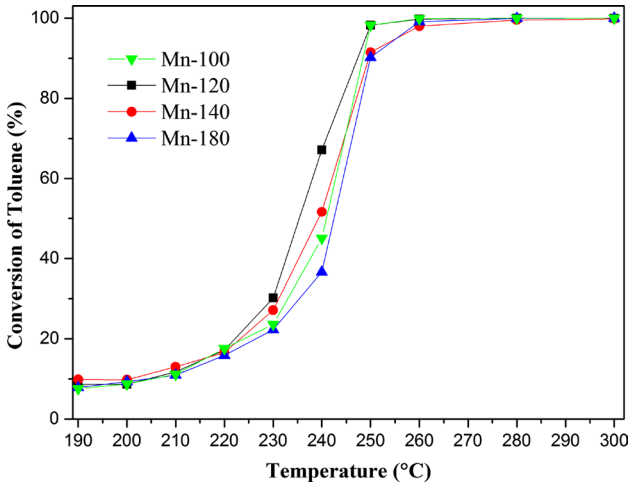

Fig. 8 Toluene conversion as a function of reaction temperature over the Mn-100, Mn-120, Mn-140 and Mn-180 catalysts under the conditions of toluene concentration = 500 ppm, 20 vol% O_2, and GHSV = 60,000 h^{-1}

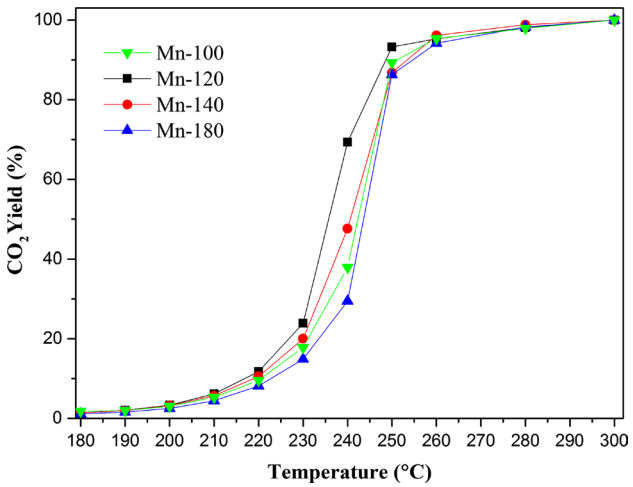

Fig. 9 CO_2 yield as a function of reaction temperature over the Mn-100, Mn-120, Mn-140 and Mn-180 catalysts under the conditions of toluene concentration = 500 ppm, 20 vol% O_2, and GHSV = 60,000 h^{-1}

main considerations in oxidation reactions which follow the MvK mechanism.

Catalytic activity tests

The performance of these catalysts in the oxidation of toluene is shown in Fig. 8, and the selectivity to CO_2 is presented in Fig. 9. As expected, the hydrothermal synthesis temperature has an important effect on the performance of MnO_x catalysts. Thus, Mn-120 showed the best catalytic activity. The values of T_{50} and T_{90} for Mn-120 were 235 and 247 °C, respectively, which are lower than those of the other three catalysts. As shown in Fig. 9, the CO_2 yields of all four samples reached over 90% at 255 °C, showing that these catalysts all possess excellent CO_2 selectivity. In addition, the yields of CO_2 showed an obvious relationship to the conversion of toluene. As previously found, the catalytic combustion of toluene proceeds in two steps [31]. This lag phenomenon arises mainly from the initial oxidation of toluene to intermediates such as benzoic acid, maleic acid and benzoic formaldehyde [31]. As the temperature was increased, the catalytic performance of the samples was enhanced, such that further oxidation occurred on the intermediates, giving CO_2 [31].

Generally, MnO_x catalysts follow the MvK mechanism in the oxidation of toluene [32]. According to this mechanism, the VOC molecules initially react with the lattice oxygen in the catalyst. The lattice oxygen is then supplemented by gaseous oxygen. Therefore, the oxygen mobility and the redox ability of the catalyst are two main factors that influence its performance. Wu et al. [33] reported that the manufacturing process can affect the catalyst's performance by modifying its morphology, oxidation state and lattice oxygen concentration. In the present case, our XRD, Raman and H_2-TPR experiments, all indicate that the Mn-120 should have the best reducibility. Besides, compared with the other three samples, a high concentration of Mn^{3+} on the surface provides more oxygen vacancies for Mn-120. Both of these considerations are essential factors for optimization of the catalytic activity. As reported by Sun [15], abundant lattice oxygen species which offer powerful oxidation ability are the main driver of increased CO_2 selectivity. Therefore, the excellent redox performance and oxygen mobility contribute to the preeminent catalytic performance of Mn-120.

Conclusions

A series of MnO_x catalysts were synthesized via hydrothermal methods at different temperatures and used for the catalytic oxidation of toluene. The different synthesis temperatures lead to changes in the microproperties and redox ability of the catalysts. Mn-120 exhibited the best catalytic activity, with 90% conversion of toluene at 247 °C. Furthermore, Mn-120 exhibited superior redox properties which can be related to smaller crystallites, higher ratios of Mn^{3+} and more lattice oxygen species, together with outstanding oxygen mobility.

Acknowledgements This work was supported by the National Natural Science Foundation of China (No. 21872096).

References

1. Yang X, Yu X, Lin M, Ma X, Ge M (2018) Enhancement effect of acid treatment on Mn_2O_3 catalyst for toluene oxidation. Catal Today. https://doi.org/10.1016/j.cattod.2018.04.041
2. Qu Z, Gao K, Fu Q, Qin Y (2014) Low-temperature catalytic oxidation of toluene over nanocrystal-like Mn–Co oxides prepared by two-step hydrothermal method. Catal Commun 52:31–35
3. Wang X, Liu Y, Zhang T, Luo Y, Lan Z, Zhang K, Zuo J, Jiang L, Wang R (2017) Geometrical-site-dependent catalytic activity of ordered mesoporous Co-based spinel for benzene oxidation: in situ DRIFTS study coupled with Raman and XAFS spectroscopy. ACS Catal 7:1626–1636
4. Li J, Tang W, Liu G, Li W, Deng Y, Yang J, Chen Y (2016) Reduced graphene oxide modified platinum catalysts for the oxidation of volatile organic compounds. Catal Today 278:203–208
5. Li L, Jing F, Yan J, Jing J, Chu W (2017) Highly effective self-propagating synthesis of CeO_2-doped MnO_2 catalysts for toluene catalytic combustion. Catal Today 297:167–172
6. Saque SM, Kondarides DI, Verykios XE (2009) Catalytic activity of supported platinum and metal oxide catalysts for toluene oxidation. Top Catal 52:517–527
7. He C, Yue L, Zhang X, Li P, Dou B, Ma C, Hao Z (2012) Deep catalytic oxidation of benzene, toluene, ethyl acetate over Pd/SBA-15 catalyst: reaction behaviors and kinetics. Asia-Pac J Chem Eng 7:705–715
8. Han Y, Ramesh K, Chen L, Widjaja E, Chilukoti S, Chen F (2007) Observation of the reversible phase-transformation of α-Mn_2O_3 nanocrystals during the catalytic combustion of methane by in situ Raman spectroscopy. J Phys Chem C 111:2830–2833
9. Wang L, Zhang C, Huang H, Li X, Zhang W, Lu M, Li M (2016) Catalytic oxidation of toluene over active MnO_x catalyst prepared via an alkali-promoted redox precipitation method. React Kinet Mech Catal 118:605–619
10. Du J, Qu Z, Dong C, Song L, Qin Y, Huang N (2018) Low-temperature abatement of toluene over Mn–Ce oxides catalysts synthesized by a modified hydrothermal approach. Appl Surf Sci 433:1025–1035
11. Wang F, Dai H, Deng J, Bai G, Ji K, Liu Y (2012) Manganese oxides with rod-, wire-, tube-, and flower-like morphologies: highly effective catalysts for removal of toluene. Environ Sci Technol 46:4034–4041
12. Cheng G, Yu L, He B, Sun M, Zhang B, Ye W, Lan B (2017) Catalytic combustion of dimethyl ether over α-MnO_2 nanostructures with different morphologies. Appl Surf Sci 409:223–231
13. Liao Y, Zhang X, Peng R, Zhao M, Ye D (2017) Catalytic properties of manganese oxide polyhedral with hollow and solid morphologies in toluene removal. Appl Surf Sci 405:20–28
14. Liao Y, Fu M, Chen L, Wu J, Huang B, Ye D (2013) Catalytic oxidation of toluene over nanorod-structured Mn–Ce mixed oxides. Catal Today 216:220–228
15. Sun H, Liu Z, Chen S, Quan X (2015) The role of lattice oxygen on the activity and selectivity of the OMS-2 catalyst for the total oxidation of toluene. Chem Eng J 270:58–65
16. Piumetti M, Fino D, Russo N (2015) Mesoporous manganese oxides prepared by solution combustion synthesis as catalysts for the total oxidation of VOCs. Appl Catal B Environ 163:277–287
17. Tang W, Wu X, Liu G, Li S, Li D, Li W, Chen Y (2015) Preparation of hierarchical layer-stacking Mn–Ce composite oxide for catalytic total oxidation of VOCs. J Rare Earth 33:62–69
18. Qi K, Xie J, Fang D, Liu X, Gong P, Li F, He F (2018) Mn_5O_8 nanoflowers prepared via a solvothermal route as efficient denitration catalysts. Mater Chem Phys 209:10–15
19. Hu F, Chen J, Peng Y, Song H, Li K, Li J (2018) Novel nanowire self-assembled hierarchical CeO_2 microspheres for low temperature toluene catalytic combustion. Chem Eng J 331:425–434
20. Kim SC, Park Y-K, Nah JW (2014) Property of a highly active bimetallic catalyst based on a supported manganese oxide for the complete oxidation of toluene. Powder Technol 226:292–298
21. Tang Q, Gong X, Zhao P, Chen Y, Yang Y (2010) Copper-manganese oxide catalysts supported on alumina: physicochemical features and catalytic performances in the aerobic oxidation of benzyl alcohol. Appl Catal A Gen 389:101–107
22. Xu J, Deng Y, Luo Y, Mao W, Yang X, Han Y (2013) Operando Raman spectroscopy and kinetic study of low-temperature CO oxidation on an α-Mn_2O_3 nanocatalyst. J Catal 300:225–234
23. Sun X, Guo R, Liu J, Fu Z, Liu S, Pan W, Shi X, Qin H, Wang Z, Liu X (2018) The enhanced SCR performance of Mn/TiO_2 catalyst by Mo modification: Identification of the promotion mechanism. Int J Hydrogen Energy 1:3. https://doi.org/10.1016/j.ijhydene.2018.07.057
24. Santos VP, Pereira MFR, Órfão JJM, Figueiredo JL (2010) The role of lattice oxygen on the activity of manganese oxides towards the oxidation of volatile organic compounds. Appl Catal B Environ 99:353–363
25. Yu D, Liu Y, Wu Z (2010) Low-temperature catalytic oxidation of toluene over mesoporous MnO_x–CeO_2/TiO_2 prepared by sol-gel method. Catal Commun 11:788–791
26. Zhang J, Li Y, Wang L, Zhang C, He H (2015) Catalytic oxidation of formaldehyde over manganese oxides with different crystal structures. Catal Sci Technol 5:2305–2313
27. Xu R, Wang X, Wang D, Zhou K, Li Y (2006) Surface structure effects in nanocrystal MnO_2 and Ag/MnO_2 catalytic oxidation of CO. J Catal 237:426–430
28. Lee SM, Park KH, Kim SS, Kwon DW, Hong SC (2012) Effect of the Mn oxidation state and lattice oxygen in Mn-based TiO_2 catalysts on the low-temperature selective catalytic reduction of NO by NH_3. J Air Waste Manag Assoc 62:1085–1092
29. Bai B, Li J, Hao J (2015) 1D-MnO_2, 2D-MnO_2 and 3D-MnO_2 for low-temperature oxidation of ethanol. Appl Catal B Environ 164:241–250
30. Chen J, Chen X, Xu W, Xu Z, Jia H, Chen J (2018) Homogeneous introduction of CeO_y into MnO_x-based catalyst for oxidation of aromatic VOCs. Appl Catal B Environ 224:825–835
31. Chen J, Chen X, Xu W, Xu Z, Chen J, Jia H, Chen J (2017) Hydrolysis driving redox reaction to synthesize Mn–Fe binary oxides as highly active catalysts for the removal of toluene. Chem Eng J 330:281–293
32. Zhang C, Wang C, Hua W, Guo Y, Lu G, Gil S, Giroir-Fendler A (2016) Relationship between catalytic deactivation and physicochemical properties of $LaMnO_3$ perovskite catalyst during catalytic oxidation of vinyl chloride. Appl Catal B Environ 186:173–183
33. Wu Y, Zhang Y, Liu M, Ma Z (2010) Complete catalytic oxidation of *o*-xylene over Mn–Ce oxides prepared using a redox-precipitation method. Catal Today 153:170–175